Chapter 2
Novel Planar Interdigital Sensors

2.1 Introduction

In this chapter, the sensor designed, modeling, simulation analysis and fabrication process will be discussed. New type of planar interdigital having unique configuration with different number of electrodes configuration will be introduced. The readers will get a good idea about design and modeling stages required to make a novel sensors. The different fabrication process involves different substrates and fabrication method will be highlighted. The main purpose of this chapter is to provide some fundamentals in the development of planar interdigital sensors.

2.2 Operating Principle

The operating principle of planar interdigital sensor basically follows the rule of two parallel plate capacitors, where electrodes open up to provide a one sided access to the material under test (MUT) [1]. The electric field lines of parallel plate capacitor and an interdigital sensor are shown in Fig. 2.1. The electric field lines generated by the sensor penetrate into the MUT and will change the impedance of the sensor. The sensor behaves as a capacitor in which the capacitive reactance becomes a function of system properties. Therefore by measuring the capacitive reactance of the sensor the system properties can be evaluated.

Since the electrodes of an interdigital sensor are coplanar, therefore the measured capacitance will give a high signal-to-noise ratio. In order to get a strong signal, the electrode pattern of the interdigital sensor can be repeated many times. The term "interdigital" refer to a digit-like or finger-like periodic pattern of parallel in-plane electrodes, used to build up the capacitance associated with the electric fields that penetrate into a material sample [1]. The conventional interdigital sensor is shown in Fig. 2.2. AC voltage source will be applied as an excitation voltage between the positive terminal and the negative terminal. An electric field is formed from positive terminal to negative terminal. Mamishev,

M. S. Abdul Rahman et al., *Novel Sensors for Food Inspection: Modelling, Fabrication and Experimentation*, Smart Sensors, Measurement and Instrumentation 10,
DOI: 10.1007/978-3-319-04274-9_2, © Springer International Publishing Switzerland 2014

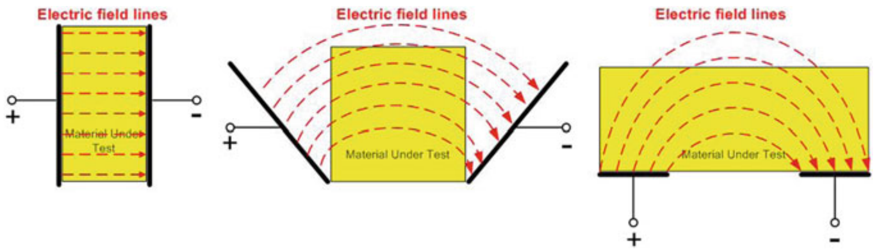

Fig. 2.1 Electric field lines of parallel plate capacitors and on coplanar interdigital sensors

Fig. 2.2 Configuration of conventional planar interdigital sensor

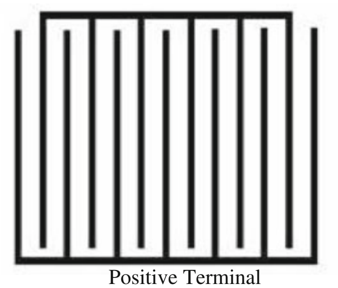

also stated that for a semi-infinite homogeneous medium placed on the surface of the sensor, the periodic variation of the electric potential along the X-axis creates an exponentially decaying electric field along the Z-axis, which penetrates the medium. Figure 2.3 illustrates Mamishev statement.

Figure 2.4 shows the side view of the interdigital sensor showing how electric field was formed between positive and negative electrodes. It is seen clearly in Fig. 2.4 that the penetration depths of the electric field lines is different for different pitch length. The pitch length of the conventional interdigital sensors is the distance between two consecutive electrodes of the same polarity. Also in Fig. 2.4, there are three pitch length (l_1, l_2 and l_3) showing the different penetration depths with respect to the pitch length of the sensor. The penetration depth can be increased by increasing the pitch length, but the electric field strength generated at the neighbouring electrodes will be weak. Planar interdigital sensors can be used for different sensing application. Figure 2.5 illustrates on the sensing possibilities of planar interdigital sensors. These sensing possibilities for various characteristic of samples have given us the opportunity to design and fabricate new type of planar interdigital sensors.

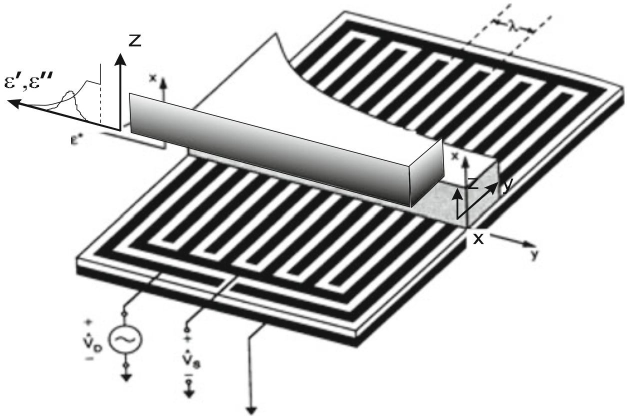

Fig. 2.3 Fringing electric field of interdigital sensor [1]

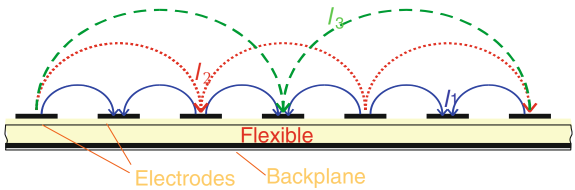

Fig. 2.4 Electric field formed between positive and negative electrodes for different pitch lengths, (l_1, l_2 and l_3) [1]

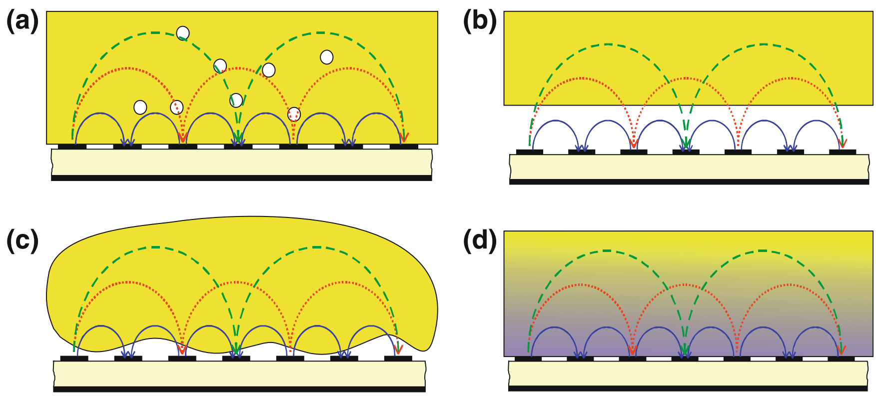

Fig. 2.5 Sensing possibilities to detect various characteristic of samples [1]. **a** sensing density, **b** sensing distance, **c** sensing texture, **d** sensing moisture

2.3 Analytical Model and Analysis

New configuration of electrode structure will be discussed in this section. The new structure was designed to have more negative electrodes in between positive electrodes. The optimum numbers of negative electrodes is an important factor to design a better performance of interdigital sensors as reported by the author in [2, 3]. More negative electrodes will result of more uniform electric filed generated within the sensors geometry. The uniformity of electric field distribution as well as higher capacitance values is two important factors in designing novel interdigital sensors.

New types of planar interdigital sensors have been designed to have better sensitivity. Three different configurations of electrode structure have been designed. The configurations of electrode structure were based on the arrangement of different numbers of positive and negative electrodes within the sensing area. These were based on the theory discussed that the numbers of negative electrodes have strong influence on distribution of electric field, penetration depth and sensing signal to create sensors with uniform electric field distribution, higher penetration depth, measurable output signal and give high sensitivity. The three configurations are 1_11, 1_5 and 1_3 which indicate that one corresponds to positive electrode and eleven, five and three are referred to negative electrodes. All designs have same electrode width, pitch length, sensing area and total numbers of electrodes (positive and negative). The combination of electrodes were designed as follows; 1-11-1, 1-5-1-5-1 and 1-3-1-3-1-3-1. The analysis of capacitance of different configurations has been conducted to study how the distribution of capacitance towards each sensor geometry.

2.3.1 Calculation of Capacitance Using Circuit Analysis

The equivalent capacitance for each sensor's geometry has been calculated in analytical way. The equivalent capacitive circuit for each sensor's geometry is shown in Fig. 2.6. All the sensors have the same area and electrodes spacing between two consecutive electrodes. The capacitors are formed between the positive and negative electrodes.

$$C = \frac{\varepsilon_0 \varepsilon_r A}{d} \tag{2.1}$$

where
C = capacitance in farads, F
ε_0 = the permittivity of free space ($\varepsilon_0 = 8.854 \times 10^{-12}$ F/m)
ε_r = the relative static permittivity or sielectric constant (vacuum = 1)
A = effective area, square meters
d = effective spacing between positive and negative electrode, meters

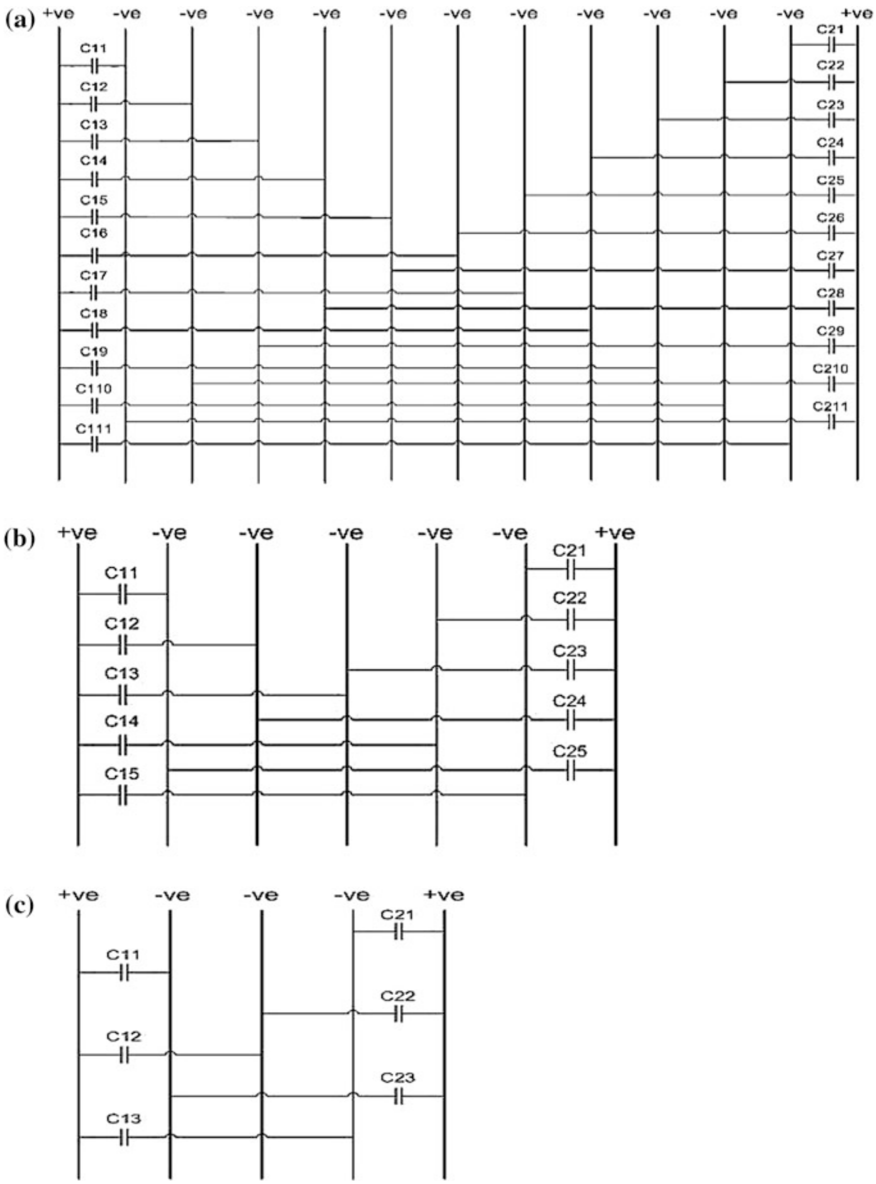

Fig. 2.6 The capacitive circuit of three different sensors; **a** 1_11 electrodes configuration (1-11-1); **b** 1_5 electrodes configuration (1-5-1-5-1) and **c** 1_3 electrodes configuration (1-3-1-3-1-3-1)

All capacitors are effectively connected in parallel. The capacitance is a function of distance between two positive and negative electrodes, d and is given by (with referenced to Fig. 2.6);

$$C_{12} = \frac{1}{2}C_{11}; \ldots C_{1n} = \frac{1}{n}C_{11} \quad (2.2)$$

and

$$C_{22} = \frac{1}{2}C_{21}; \ldots C_{2n} = \frac{1}{n}C_{21} \quad (2.3)$$

where $C_{11} = C_{21}$; C_{11} is the capacitance between the positive electrode and closest negative electrode.

Therefore the total equivalent capacitance (C_{eq}) for each sensor's geometry is given by;

$$C_{eq(1)} = C_{11} + C_{12} + \ldots C_{1n} \quad (2.4)$$

$$C_{eq(2)} = C_{21} + C_{22} + \ldots C_{2n} \quad (2.5)$$

where $C_{eq(1)}$ is for equivalent capacitance in the first geometry of each sensor while $C_{eq(2)}$ is the equivalent capacitance in the second geometry of each sensor.

Therefore total capacitance within sensor geometry is given by;

$$C_{Total} = C_{eq(1)} + C_{eq(2)} \ldots + C_{eq(n)} \quad (2.6)$$

The estimated capacitance within each sensor's geometry is shown in Fig. 2.7. It is shown that Sensor 1_11 has better uniformity in terms of distribution of effective capacitance throughout the sensors geometry compared to Sensor 1_5 and Sensor 1_3, but has lower total capacitance value. The result from analytical analysis is in line with the result shown in the simulation using COMSOL. It is important to achieve better sensitivity in terms of uniform distribution of total capacitance value and the uniformity of electric field distributions throughout the sensor geometry. The performance of the sensors depends on the characteristic of the sensor and also the characteristic of the material under test (MUT). Therefore the experiments of sensors with MUT will determine the best sensing performance of different sensor configurations.

2.4 Modelling Using Finite Element Analysis: COMSOL Multiphysics

Finite element analysis is a computational program used to study and analyse model of material or design. Finite element analysis has been used widely for modelling of planar interdigital sensors for various applications [4–7]. The COMSOL Multiphysics® (formerly FEMLAB) is a finite element analysis and solver software package for various physics and engineering applications, especially coupled phenomena, or multiphysics. The software applications are based on partial differential equations (PDEs) [8]. The sensors were modelled to derive the optimum structure of sensor for better performance. The Electromagnetic module

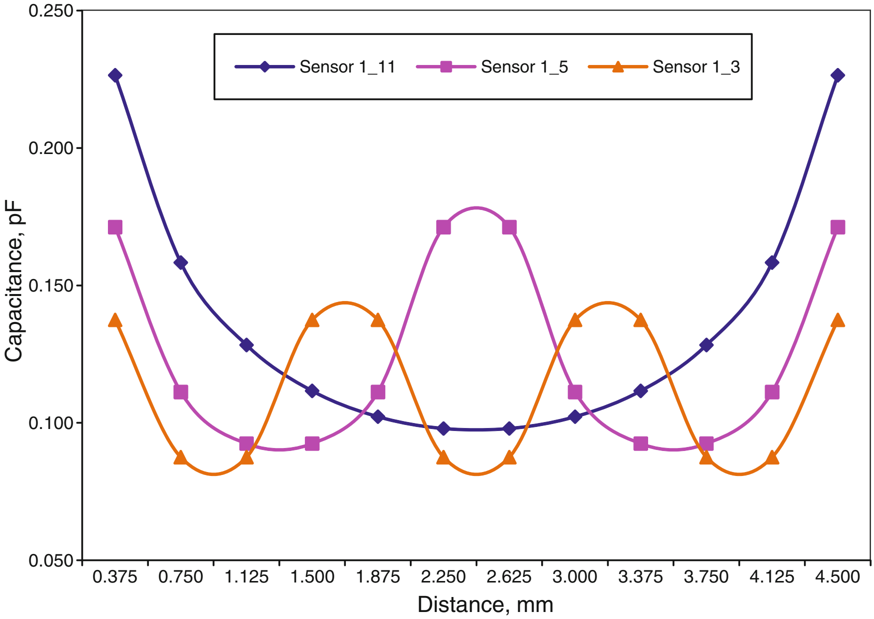

Fig. 2.7 Equivalent capacitance within each sensor geometry

of COMSOL was used for analysis of novel interdigital sensors. The application was in 3D and AC/DC module for electrostatics mode for dielectric material was selected. Figure 2.8 shows the arrangement of positive electrodes and negatives electrodes of the sensor design in 3D view. The sensors were modelled using the actual size of the fabricated sensors. COMSOL Multiphysics has been used to characterize the planar meander sensor and interdigital sensor as discussed in [9] and [10]. This following section will discuss in detail the capability of the COMSOL Multiphysics to simulate and analyse the novel planar interdigital sensors.

2.4.1 Model Definition: COMSOL Implementation

The analysis using COMSOL was carried out to observe how optimum number of negative electrodes between two positive electrodes of interdigitated configuration contributes to highest sensitivity measurement. Analysis was conducted for different number of negative electrodes between two positive electrodes. All electrodes were modeled to have the same pitch (250 μm), same electrode length (4,750 μm), electrode width (125 μm) and same sensing area configurations.

The capacitance value of each sensor design can be calculated from COMSOL applications. The value for electrostatic energy density, W_e can be obtained from

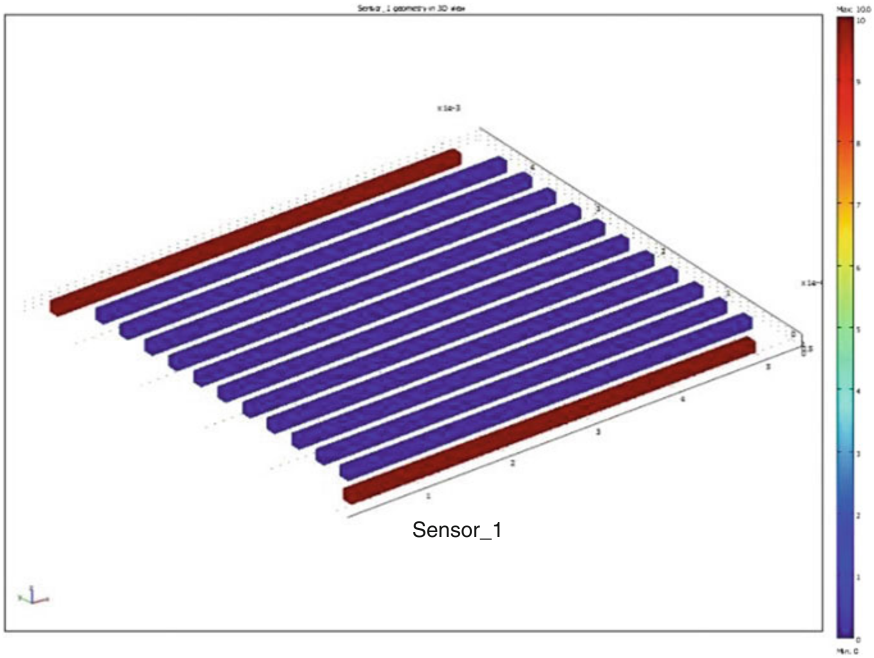

Fig. 2.8 The geometry of interdigital sensor in 3D view

the simulation. The energy required to charge a capacitor should equal that of the electrostatic field, which is given by;

$$W_e = \frac{Q^2}{2C} \tag{2.7}$$

W_e is available in the Electrostatics application mode; the software calculates it by integrating across the domain

$$W_e = \int_{\Omega} (D.E) d\Omega \tag{2.8}$$

where, D is the electric displacement, E is the electric field intensity and $d\Omega$ is the domain boundary. The capacitance, C, is related to the charge on the two conductive plates, Q, and the voltage difference across those plates, ΔV, by;

$$C = \frac{Q}{\Delta V} \tag{2.9}$$

The calculation of C is carried out from the stored electric energy, $W_{e,}$ and the voltage across the two plates, ΔV, and is given by;

$$C = \frac{Q^2}{2W_e} = \frac{C^2 \Delta V^2}{2W_e} \Rightarrow C = \frac{2W_e}{\Delta V^2} \tag{2.10}$$

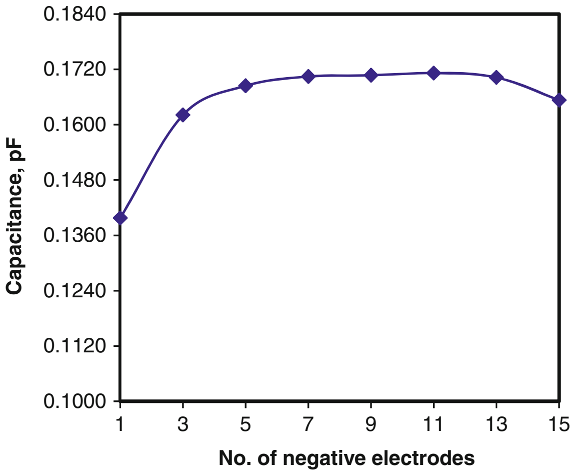

Fig. 2.9 The relationship between Capacitance and no. of negative electrodes

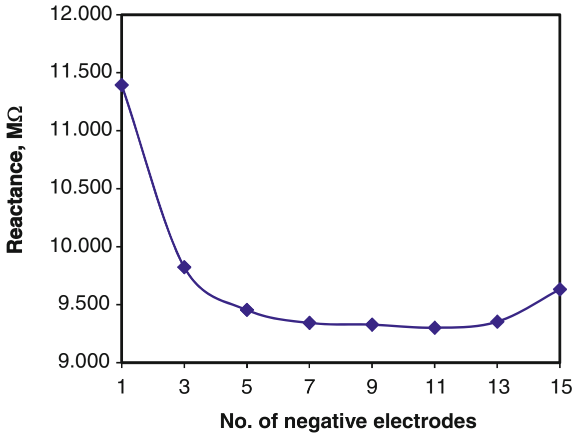

Fig. 2.10 The relationship between Reactance and no. of negative electrodes

Therefore,
$$C = \frac{2W_e}{\Delta V_0^2} \tag{2.11}$$

where; W_e is the stored electrostatic energy density and V_0 is the applied voltage to the positive electrode. The negative electrode is kept at 0 V.

The calculated capacitance and reactance as a function of number of negative electrodes between two positive electrodes obtained from simulation are shown in Figs. 2.9 and 2.10 respectively. It was observed that the number of negative electrodes between 5 and 13 has the highest capacitance and consequently the lowest reactance value. This is true since from Eq. (2.1) the capacitance only depends on effective area (A) as other parameters remain constant (ε_0, ε_r and d). Therefore, as the number of negative electrodes increase the effective area (A) also

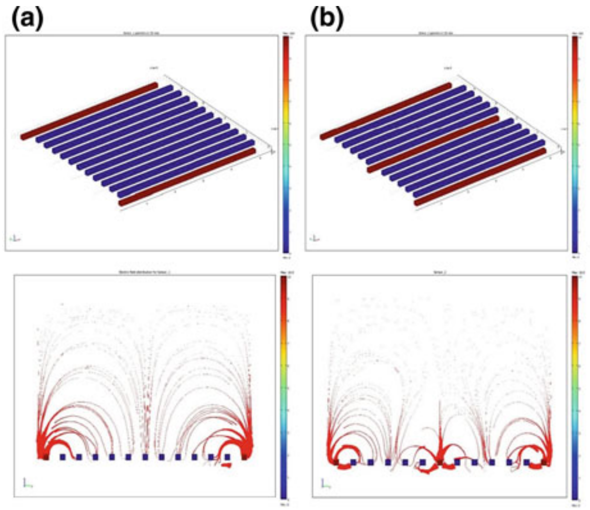

Fig. 2.11 Electric field distribution of each sensors; **a** Sensor 1_11, **b** Sensor 1_5 and **c** Sensor 1_3

increase and consequently the capacitance increases. This is only true for certain number of negative electrodes as with the increase number of negative electrodes, the electric field strength becomes weak and the capacitance is reduced.

Further analysis was conducted to evaluate the distribution of electric field and to measure the electric field intensity for all three sensors. Figure 2.11 shows the simulation results of electric field distribution of each sensor. As for Sensor 1_11, the magnitude of electric field strength is stronger at neighbouring electrodes but as it goes to the middle it becomes weak. It is also shown in Fig. 2.11 that the electric field strength becomes weak as it goes up. The same results were observed from the simulation results of Sensor 1_5 and Sensor 1_3 having different configuration. It is shown that optimum numbers of negative electrodes between positive electrodes will give better distribution of electric field but comparatively weak in field strength. The electric field strength needs to be sufficient to interact with material under test.

The variation of electric field intensity was then analysed for each sensor designed. Electric field intensity is a measurement of electric field (V/m) along the z-axis. The cross-section line data were set starting from coordinates $X_0 = 2.75$ mm, $Y_0 = 0$ mm, $Z_0 = 0.125$ mm and $X_1 = 2.75$ mm, $Y_1 = 4.75$ mm, $Z_1 = 0.125$ mm. The coordinate of Z_0 and Z_1 were replaced from 0.125 to 3.50 mm and electric field intensity data were recorded. The average of electric field intensity is shown in Fig. 2.12. Sensor 1_11 has been chosen for analysis. Table 2.1 shows the calculated capacitance value of each sensor measured from the simulation.

Sensor 1_11 was chosen for further analysis using COMSOL. The analysis was conducted by placing sample into the model. Two analyses have been conducted. The first analysis was to observe the relationship of capacitance for different values

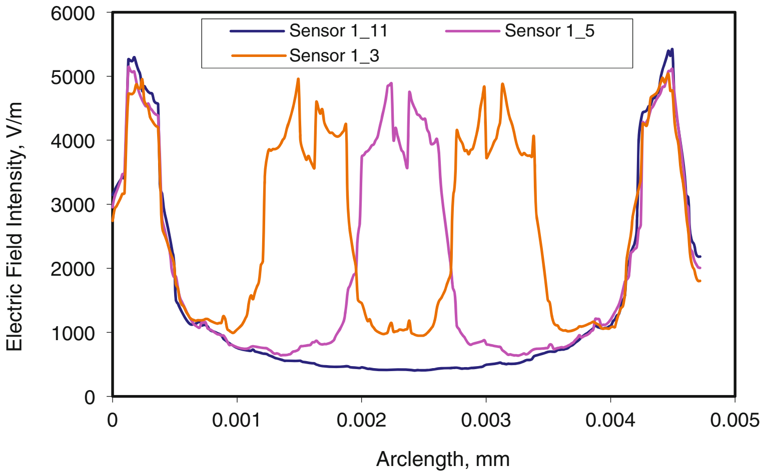

Fig. 2.12 Electric field intensity of each sensor

Table 2.1 Calculated capacitance from the modelling using COMSOL multiphysics for inter-digital sensors

Sensor type	Simulation parameters			Calculated parameters
	V_e (V)	Frequency (kHz)	Electrostatic energy density (J)	Capacitance (pF)
Sensor 1_11	10.0	10.0	8.5421×10^{-11}	1.709
Sensor 1_5	10.0	10.0	1.3823×10^{-11}	2.765
Sensor 1_3	10.0	10.0	1.7091×10^{-10}	3.418

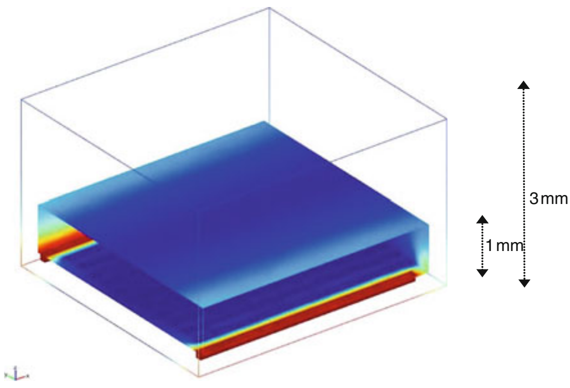

Fig. 2.13 3D view of Sensor 1_11 with a known sample

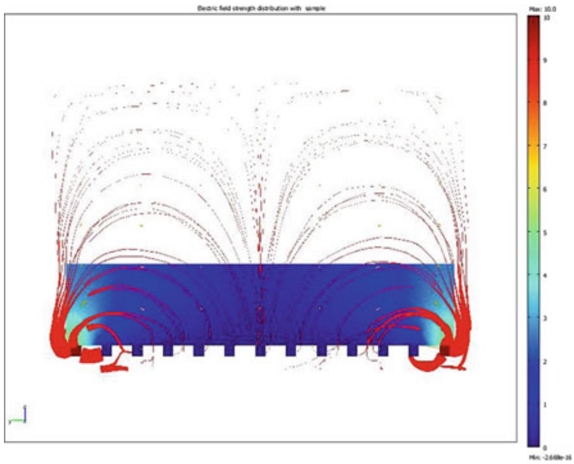

Fig. 2.14 Electric field distribution of Sensor 1_11 for a known sample

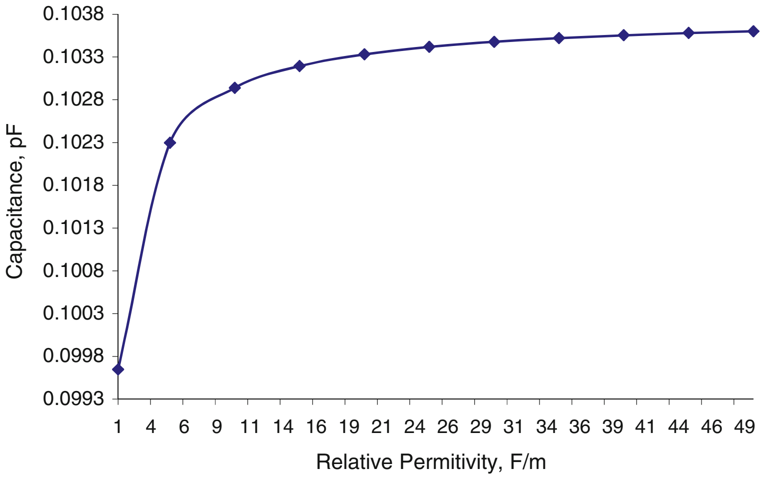

Fig. 2.15 Calculated capacitance for different values of sample permittivity

of effective permittivity (ε_r) of sample while maintaining the same thickness (1 mm). The second analysis was to evaluate the capacitance produced by the sensor with different sample thickness while keeping the permittivity value constant (air gap, $\varepsilon_r = 1$ and sample, $\varepsilon_r = 3.6$). The 3D model for the analysis is shown in Fig. 2.13. The model consists of Sensor 1_11, a sample and a box with constant height of 3 mm (enclosed system). The electric field passing through the sample and the effect of permittivity of sample and air is shown in Fig. 2.14. From Fig. 2.15, it is seen that the capacitance has increased with the increase in

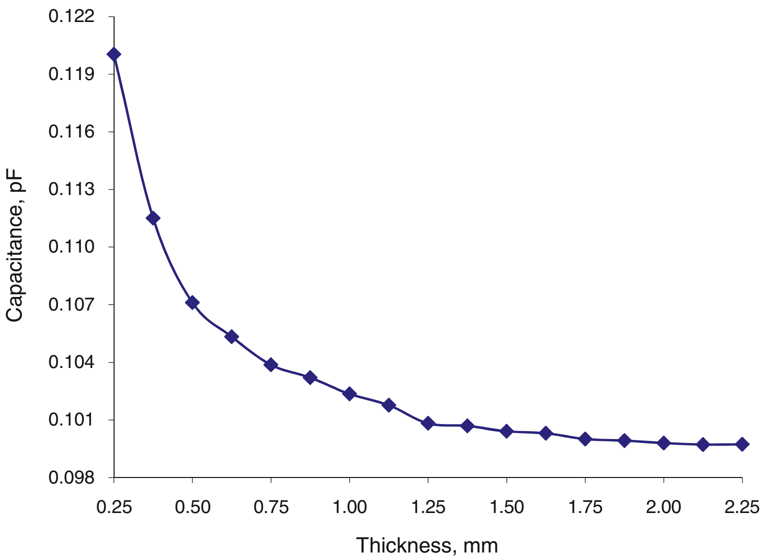

Fig. 2.16 Calculated capacitance for different values of sample thickness

permittivity of the sample. The increase of capacitance is not proportional to sample permittivity due to significant influence of air. Result in Fig. 2.16 shows that the capacitance value decrease as the sample thickness increases.

2.5 Design and Fabrication Process

Initial design on the sensors was done using Altium Designer 6 software. The final design of each sensor from the Altium Designer was printed in negative and then was transferred into a film. The conducting layers of the board are typically made of thin copper foil. The insulating layers (dielectric) are typically laminated together with epoxy resin pre-impregnated. The film together with the board was exposed to the UV light. This process will impress and burn the desired sensor design onto the board. The printed circuit was developed. The printed circuit board was immersed into a chemical for etching process to remove the unwanted copper, leaving only the desired copper trace. The sensor was cut to a desired design to make it suitable for testing.

2.5.1 Conventional Interdigital Sensors

Initial part of the research works were involved design and fabrication of three conventional planar interdigital sensors. The initial goal is to understand how

Table 2.2 Conventional interdigital sensor parameters

Sensor	Sensing area (mm^2)	Pitch length (mm)	Number of electrodes	
			Positive	Negative
Din_10mil	25	0.25	5	6
Din_20mil	25	0.51	4	4
Din_40mil	25	1.02	2	3

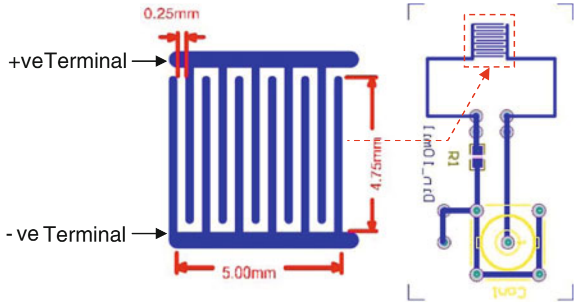

Fig. 2.17 Representation of conventional interdigital sensor with configuration #1

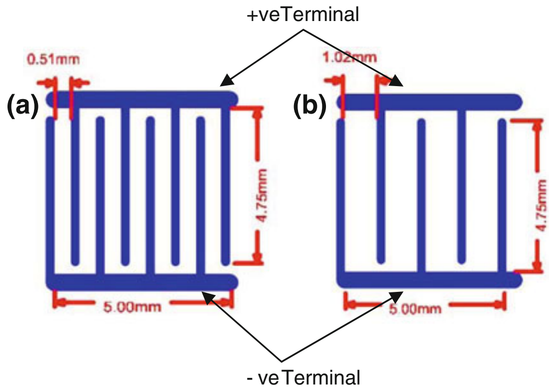

Fig. 2.18 Conventional sensor with **a** Configuration #2 and **b** Configuration #3

conventional interdigital sensor works and respond to materials. All three sensors were designed with different configurations, so that the difference of their response can be evaluated. Each sensor was designed to have same effective area of 5,000 by 5,000 µm but with different pitch lengths of 250, 510 and 1,020 µm. The negative and positive electrodes have the same length of 4,750 µm and width of 250 µm. Table 2.2 shows the parameters for conventional interdigital sensors. Figure 2.17 shows the representation of conventional interdigital sensor with configuration #1 (Din_10mil) and Fig. 2.18 shows the representation of conventional interdigital sensor with configuration #2 (Din_20mil) and configuration #3 (Din_40mil). Figure 2.19 shows the fabricated conventional interdigital sensors.

Fig. 2.19 The fabricated conventional interdigital sensors compared to 20¢ New Zealand coin

2.5.2 Novel Planar Interdigital Sensors

Novel planar interdigital sensors were developed to have better sensitivity measurement with better response to material under test. The design of novel planar interdigital sensors is unique because they are different compared to conventional interdigital sensors. The uniqueness of the novel sensors because they were designed to have more negative electrodes in between positive electrodes with different configurations of electrode structure. All sensors were designed to have same effective area of 4,750 by 5,000 μm and having pitches of 250 μm. The positive and negative electrodes have the same length and width of 4,750 and 125 μm respectively. The sensors were fabricated on three different materials with different fabrication process.

2.5.2.1 FR-4 Sensors

The initial sensors were fabricated on FR4 using normal printed circuit board technology. All sensors have equal numbers of electrodes (thirteen). The only parameter changing in the sensor design is the *d*, spacing between two adjacent positive and negative electrodes between which the electric field-lines exist. Sensor 1_11 was designed to have two positive electrodes at each end separated by eleven negative electrodes. Sensor 1_5 and Sensor 1_3 were designed with the same dimensions but with different configurations. Sensor 1_5 has five negative electrodes between two positive electrodes and has the same pitch like Sensor 1_11. Sensor 1_3 has three negative electrodes between two positive electrodes. Table 2.3 shows the parameters for novel interdigital sensors. Figure 2.20 shows the representation of sensor configuration #1 (Sensor 1_11). Figure 2.21 shows sensor configuration #2 (Sensor 1_5) and sensor configuration #3 (Sensor 1_3). The fabricated novel interdigital sensors are shown in Fig. 2.22.

Table 2.3 Novel interdigital sensor parameters

Sensor	Sensing area (mm^2)	Pitch length (mm)	Number of electrodes	
			Positive	Negative
Sensor 1_11	23.75	0.125	2	11
Sensor 1_5	23.75	0.125	3	10
Sensor 1_3	23.75	0.125	4	9

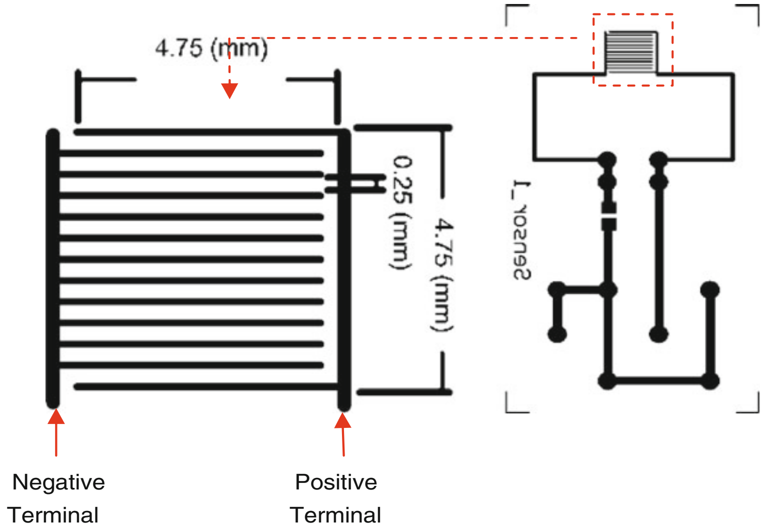

Fig. 2.20 Representation of Sensor 1_11 configuration

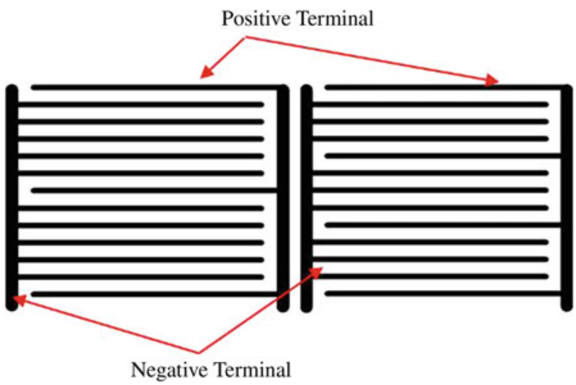

Fig. 2.21 Sensor 1_5 and Sensor 1_3 with different configurations

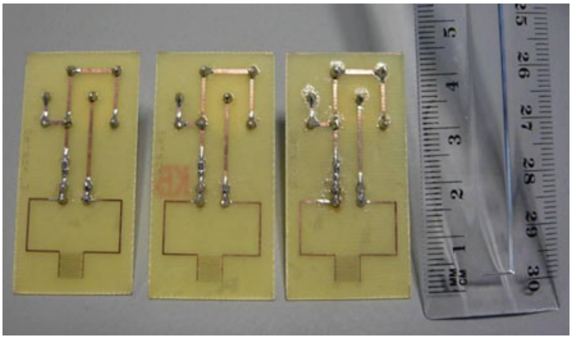

Fig. 2.22 The fabricated novel interdigital sensors (FR4)

2.5.2.2 Alumina Sensors

The second sensors were fabricated on alumina as its platform. The sensors were constructed using standard thick film printing methodologies. The pattern was drawn in AutoCad and then printed on a Fire 9,500 photoplotter. The patterns were then transferred to three 325 mesh screens. The printer used in the fabrication was a Presco 435, which is capable of printing up to a 100 mm × 100 mm substrate. The top trace layer was printed using a PdAg 850 °C firing alloy while the ground plane was made using a 850 °C silver material. The solder dam was made using a 600 °C of low k dielectric to prevent solder bridging. The wet paste was dried and fired after each individual layer was printed. The paste was dried at 150 °C then was inspected consistently. The dried substrate was then placed on the belt of a BTU firing furnace profiled to deliver 850 °C ± 5 °C for 10 min. The duration of the entire firing cycle is approximately 30 s. The substrates were then patterned for the next layer and the cycle was repeated. The final layer is a low k dielectric to limit the solder flow during the mounting of a chip resistor. Figure 2.23 shows the design of fabricated sensors which were fabricated at Northern Illinois University, United States. Figure 2.24 shows the fabricated sensors.

2.5.2.3 Glass Sensors

The third sensors were fabricated on glass using MEMS technology. The plastic photo mask design was used because of low cost and easy to prepare. The glass slip (sensor platform) was first cleaned with acetone. Then, an ultrasonic cleaning machine was used to clean the glass in methanol solution. N_2 gun was used to dry the glass slide. The IDT electrode fabrication process starts by depositing the Cr or Au on the glass slide using E-beam evaporated machine. Then, the positive photo-resist (PR) was coated on the metal layer by using spin coater. The coated metal

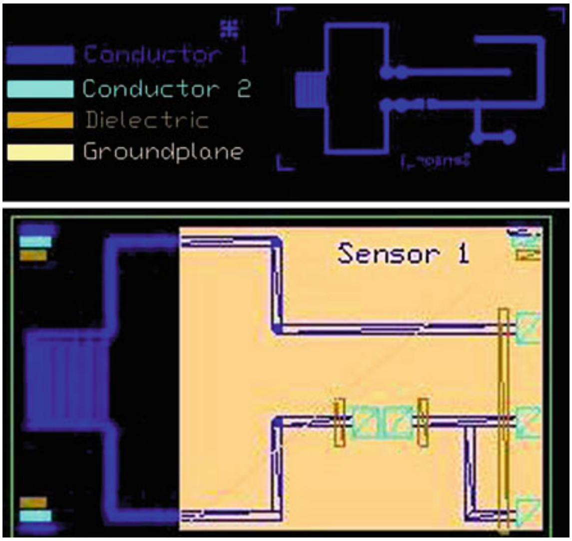

Fig. 2.23 The representation of interdigital sensor (Sensor 1_11)

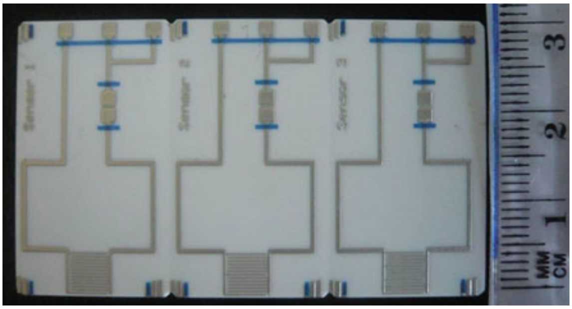

Fig. 2.24 The fabricated interdigital sensors (Alumina)

layer was exposed to the UV light. The Developer machine was used to remove the unexposed PR.

The etching process was done to remove the surplus metal and also to remove the remaining PR leaving only the patterned electrode. Figure 2.25 shows the IDT electrode fabrication process. Figure 2.26 shows the representation of interdigital sensor which were using MEMS and have been fabricated at Southern Taiwan University, Taiwan. Figure 2.27 shows the fabricated interdigital sensors using MEMS technology. Figure 2.28 shows the three different designs of fabricated novel interdigital sensors.

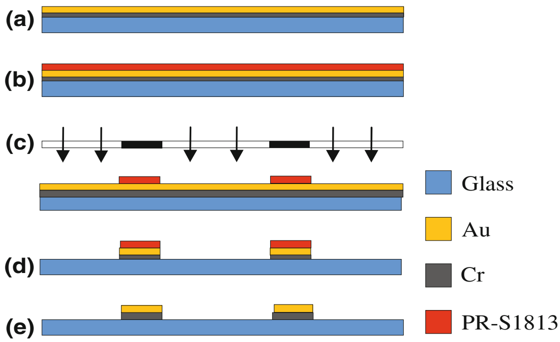

Fig. 2.25 The IDT electrode fabrication process. **a** deposit Au/Cr layer, **b** coat PR—S1813, **c** expose and develop, **d** etching electrode, **e** remove PR

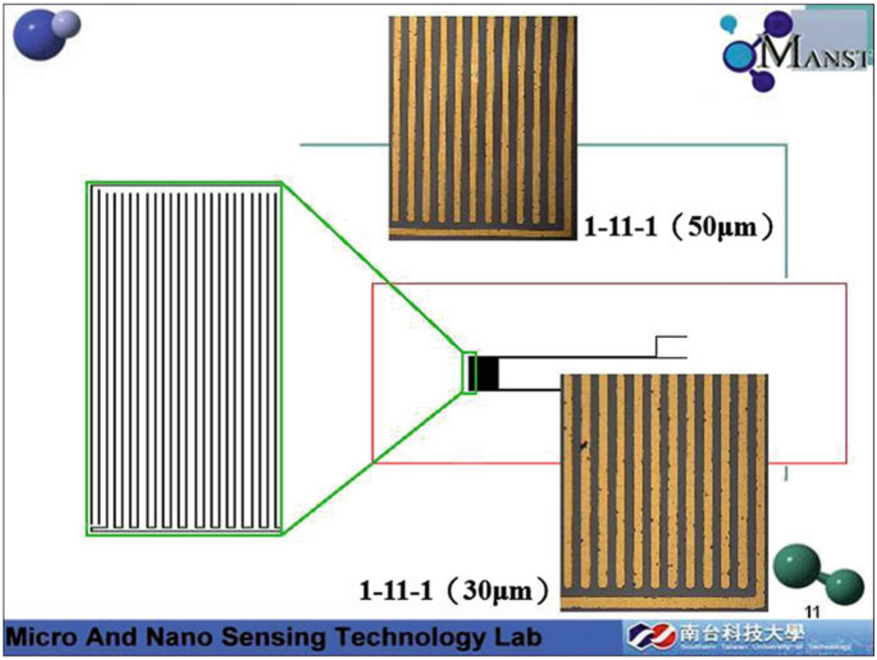

Fig. 2.26 The representation of interdigital sensor (Glass)

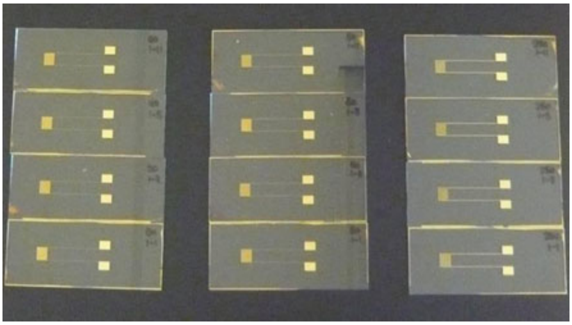

Fig. 2.27 The fabricated interdigital sensors using MEMS technology

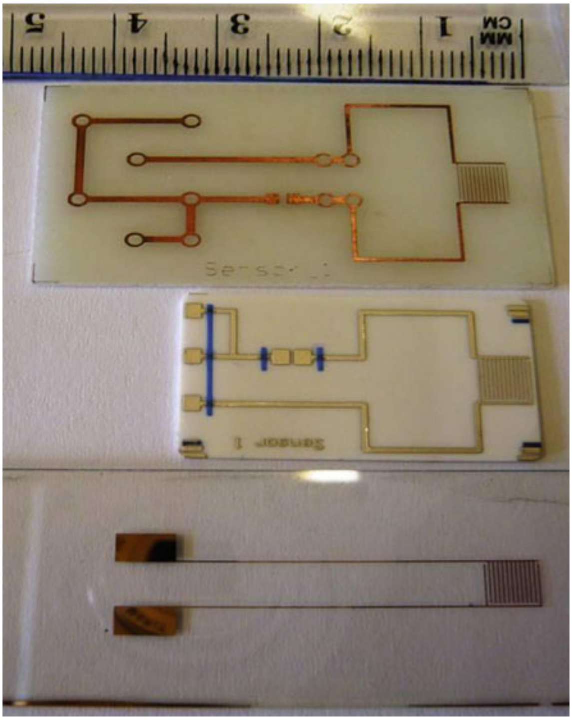

Fig. 2.28 The representation of three different designs of novel interdigital sensors

2.5.2.4 Silicon Sensors

The latest design of the thin film planar interdigital structure was fabricated by photolithography and etching techniques on a Silicon/Silicon Dioxide (Si/SiO_2) wafer (single side polished). The schematic diagram of electrode configurations is shown in Fig. 2.29. Figure 2.30 shows the fabrication process of the new silicon sensors. The sensor was fabricated to have multiple configurations of 1_11, 1_5 and 1_3. The sensors are designed to have better output signal, low impedance and

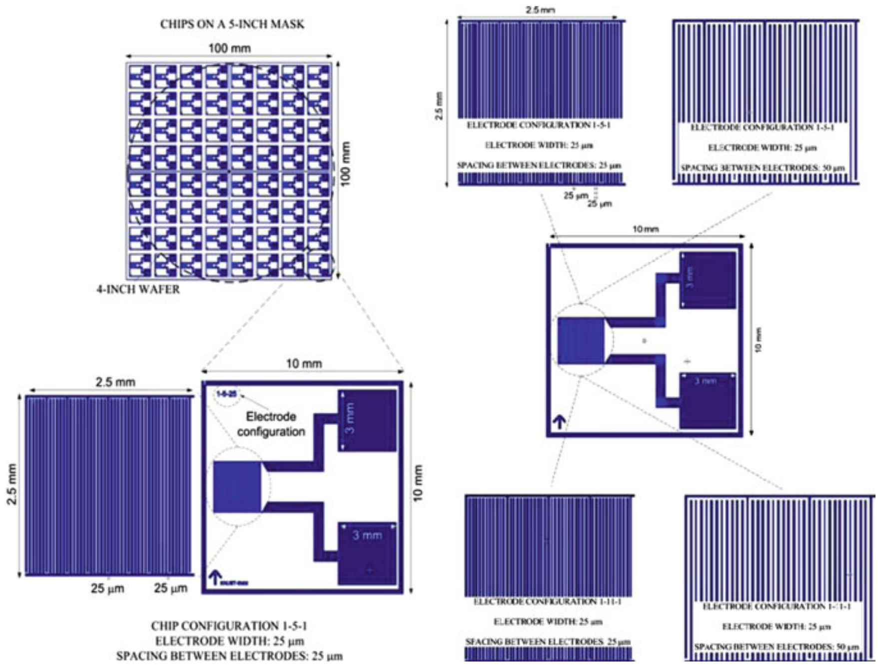

Fig. 2.29 Interdigital electrode configurations

improved sensitivity. The fabricated dies have a rigid substrate which is advantageous in noncontact measurements. In order to implement model-based parameter estimation algorithms effectively it is important to maintain a well-defined geometry of the electrode structure. CoventorWare was used to design the patterns of the ID structures. The patterns varied according to the spatial wavelength of the periodic interdigital strucuture while the width of electrodes and the sensing area was set to constant values of 25 µm and 2.5 mm × 2.5 mm respectively.

All patterns were printed on a 5 inch soda lime transparent mask using a mask laser writer. Pre-baking was performed at 150 °C on the wafer substrate so that the photoresist attached better to the surface. A spin coater was used to coat 4 m of positive photoresist (EC13027) on a 4 inch wafer. An oven was used to post bake the wafer at 100 °C for 1 min. A UV light exposure tool was used to transfer the ID patterns to photoresist of the wafer. A constant dose of 200 mJ/cm^3 was used at a separation of 30 µm between the wafer and the mask. The wafer was then developed for 1 min under a solution Tetra-Methyl Ammonium Hydroxide (TMAH) based solution (AZ 726). Plasma ashing at 70 °C was used to perform a "Descum" process to remove residual photoresist in trenches. Following this, 20 nm of Chromium (Cr) and 500 nm of Gold (Au) in which the latter acts as a barrier layer for good adhesion, were sputtered on to the wafer substrate by DC magnetron sputtering. Gold electrodes have the advantage of being inert and

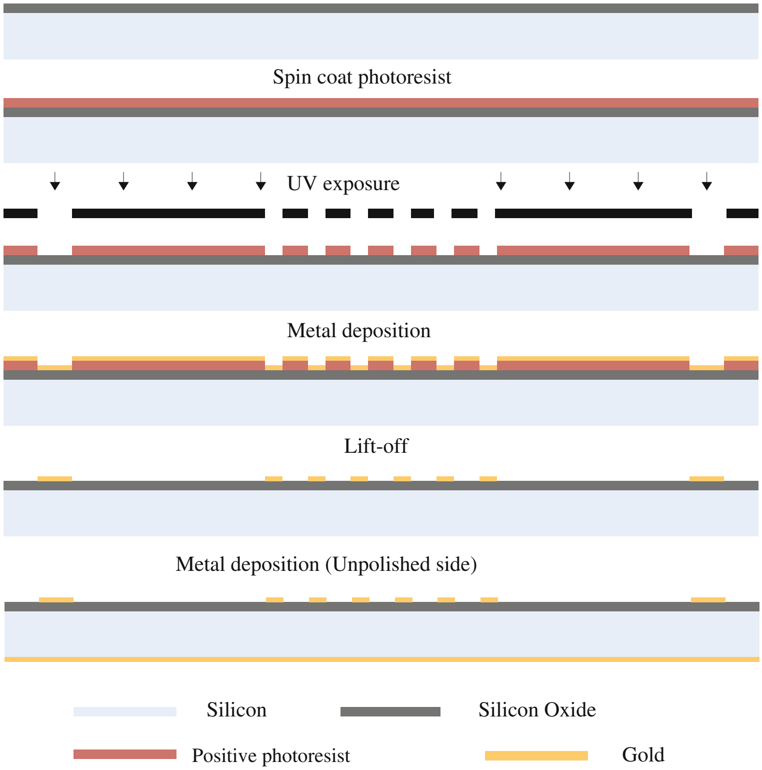

Fig. 2.30 The fabrication process on silicon wafer (Mask 1)

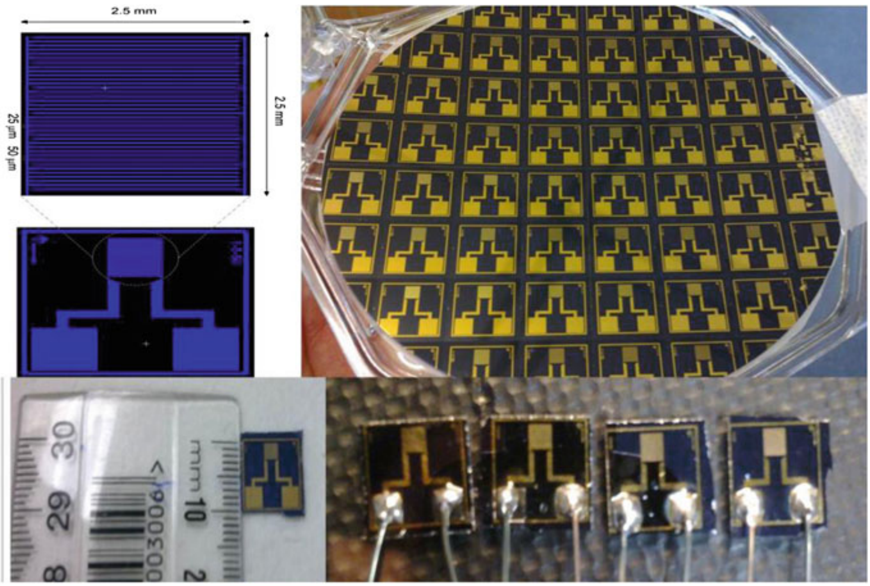

Fig. 2.31 Thin film silicon interdigital sensor

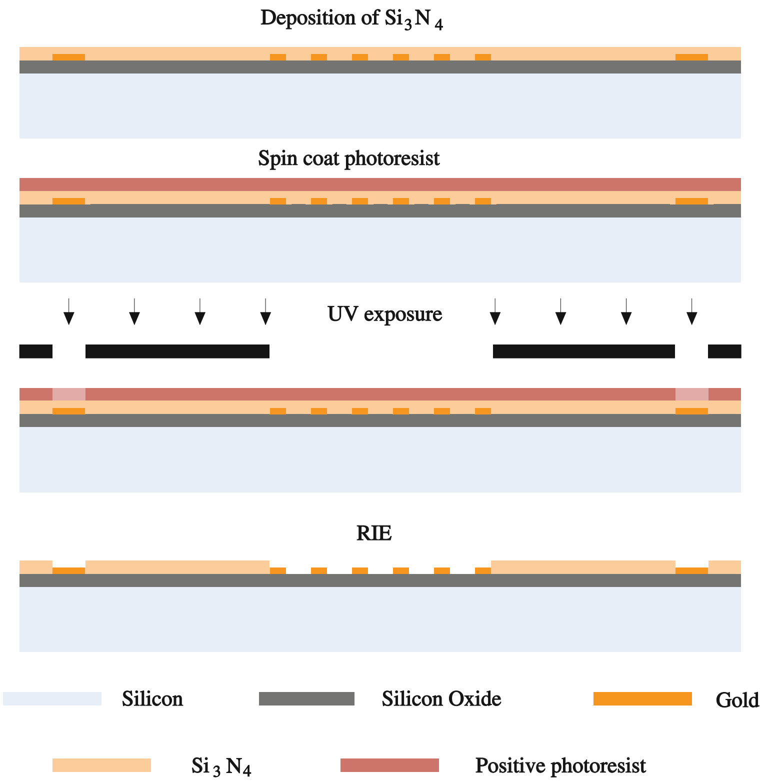

Fig. 2.32 Fabrication process (Mask 2—Deposition of Si_3N_4 by PECVD and etching by RIE)

flexible. Argon gas was used at a pressure of 30 mTorr and the DC power was set to 800 W. Lift-off was then performed under a solution of acetone. After lift-off, the unpolished side of the wafer was also sputtered with 20 nm of Chromium (Cr) and 500 nm of Gold (Au). This will act as the guard plane. A follower op-amp can drive the guard plane to be equal to the sensing voltage hence eliminating any current between the sensing and guard electrodes through the substrate. Thus, the conductance and capacitance between the sensing and guard plane are eliminated, leading to simplified response analysis and improved device sensitivity. The fabricated silicon based interdigital sensor is shown in Fig. 2.31.

An improved design of the silicon sensors has been fabricated. The initial fabrication process is the same for Mask 1 as in Fig. 2.30. The improved part was in fabrication of Mask 2 as shown in Fig. 2.32. After lift-off, the wafer was coated with a 200 nm layer of Silicon Nitride (Si_3N_4) by plasma enhanced chemical vapor deposition (PECVD). Si_3N_4 has been used in many microdevices as a passivation layer since its film properties can be easily controlled and modified by varying its deposition methods and conditions. Moreover, Si_3N_4 can withstand continuous exposure to air at high temperatures for long periods of time. The deposition of

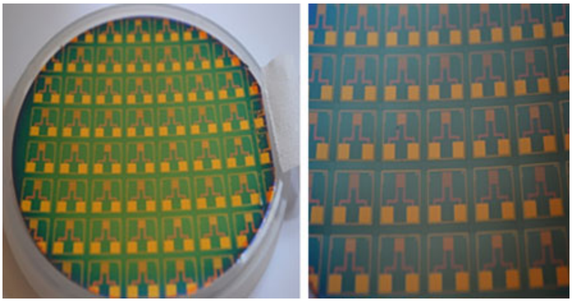

Fig. 2.33 Newly improved silicon based interdigital sensor

Si_3N_4 using the PECVD technique results in films that have good adhesion, low pinhole density, good step coverage and uniformity. All areas except the electrodes and bonding pads were covered with Si_3N_4. Since the electrodes are open complementary biomolecules can be coated directly on top of the electrodes. This way target biomolecules will be attached as close as possible to the electrodes leading to high detection signals.

After Si_3N_4 coating 4 μm of positive photoresist (EC13027) was coated on the wafer. A UV light exposure tool was used to soften the resist over the electrodes and bonding pad windows. After development reactive ion etching (RIE) was used to open the area with electrodes and the bonding pads. RIE is one method of dry etching and it prevents the undercutting cause by wet etching. In dry etching an anisotropic etches is created. An anisotropic etch is critical for high-fidelity pattern transfer. The latest silicon sensors is shown in Fig. 2.33.

References

1. A.V. Mamishev, K. Sundara-Rajan, F. Yang, Y.Q. Du, M. Zahn, Interdigital sensors and transducers. Proc. IEEE **92**, 808–845 (2004)
2. A.R. Mohd Syaifudin, K.P. Jayasundera, S.C. Mukhopadhyay, Initial investigation of using planar interdigital sensors for assessment of quality in seafood. Hindawi J. Sens. **2008**, 9 (2008)
3. A.R.M. Syaifudin, K.P. Jayasundera, S.C. Mukhopadhyay, A low cost novel sensing system for detection of dangerous marine biotoxins in seafood. Sensor Actuat. B-Chem. **137**, 67–75 (2009)
4. C.R. Bowen, A. Bowles, S. Drake, N. Johnson, S. Mahon, Fabrication and finite element modelling of interdigitated electrodes. Ferroelectrics **228**, 257–269 (1999)
5. L.A. Ramajo, D.E. Ramajo, M.M. Reboredo, D.H. Santiago, M.S. Castro, Evaluation and modelling of integral capacitors produced by interdigitated comb electrodes. Mater. Research-Ibero-American J. Mater. **11**, 471–476 (2008)
6. A.K. Sen, J. Darabi, Modeling and optimization of a microscale capacitive humidity sensor for HVAC applications. IEEE Sens. J. **8**, 333–340 (2008)
7. M.S. Webster, I.V. Timoshkin, S.J. MacGregor, M. Mattey, Computer Aided Modelling of an interdigitated microelectrode array impedance biosensor for the detection of bacteria. IEEE Trans. Dielectr. Electr. Insul. **16**, 1356–1363 (2009)

8. COMSOL, *COMSOL Multiphysics: Modelling Guide*, COMSOL 3.5a edn. (COMSOL AB, 2008)
9. S.C. Mukhopadhyay, C.P. Gooneratne, G. Sen Gupta, S. Yamada, Characterization and comparative evaluation of novel planar electromagnetic sensors. IEEE Trans. Magn. **41**, 3658–3660 (2005)
10. A.R. Mohd Syaifudin, S.C. Mukhopadhyay, P.L. Yu, Modelling and fabrication of optimum structure of novel interdigital sensors for food inspection. Int. J. Numer. Model. Electron. Networks Devices Fields **25**(1), 64–81 (2012). doi:10.1002/jnm.813

http://www.springer.com/978-3-319-04273-2

Novel Sensors for Food Inspection: Modelling, Fabrication and Experimentation

Abdul Rahman, M.S.; Mukhopadhyay, S.C.; Yu, P.L.

2014, IX, 140 p. 152 illus., 134 illus. in color., Hardcover
ISBN: 978-3-319-04273-2